Appl Petrochem Res (2016) 6:73–87
DOI 10.1007/s13203-015-0136-8

ORIGINAL ARTICLE

Catalytic functionalities of nano Ru catalysts supported on TiO_2–ZrO_2 mixed oxide for vapor phase hydrogenolysis of glycerol to propanediols

Vanama Pavan Kumar[1] · Jorge N. Beltramini[2] · Samudrala Shanthi Priya[1,3] · Amirineni Srikanth[1] · Ponnala Bhanuchander[1] · Komandur V. R. Chary[1]

Received: 13 March 2015 / Accepted: 11 August 2015 / Published online: 29 August 2015

Abstract Vapor phase hydrogenolysis of glycerol was studied over Ru catalysts supported on TiO_2–ZrO_2 binary oxide. Ru catalysts with various ruthenium loadings from 1.0 to 6.0 wt% were prepared by deposition–precipitation method on the TiO_2–ZrO_2 mixed oxide support. These catalysts were characterized by X-ray diffraction, H_2 temperature-programmed reduction, NH_3 temperature-programmed desorption, transmission electron microscopy, BET surface area, XPS and CO chemisorption measurements. The catalysts exhibited superior performance for the vapor phase hydrogenolysis of glycerol at moderate temperature and atmospheric pressure. The mixed oxide support plays a significant role in improving the catalytic activity for the production of propanediols. The glycerol conversion and the selectivity of various products depend on the catalyst preparation method and also on the Ru content. The influence of acidity of the catalyst and its correlation to the catalytic performance (selectivity and conversion) has been studied. The weak and strong acidic sites of the catalysts measured by NH_3-TPD play a key role in selective formation of 1,2-propanediol and 1,3-propanediol. XRD, TEM, XPS and CO chemisorption studies revealed that ruthenium was well dispersed on TiO_2–ZrO_2 which further contributed to the superior catalytic activity for glycerol hydrogenolysis.

Keywords Glycerol hydrogenolysis · Ruthenium · Titania–Zirconia · 1,2-Propanediol · 1,3-Propanediol

Introduction

Glycerol acts as a top building block that probably serves as an important biorefinery feedstock [1, 2]. In addition, it is a byproduct from the production of biodiesel from vegetable oils [3]. Conversion of glycerol into valuable chemicals by a green catalytic process is a challenging area of present research. Glycerol is normally generated at the rate of 1 mol for every 3 mol of methyl esters synthesized [4]. Hydrogenolysis of glycerol is a catalytic chemical reaction that breaks a chemical bond in an organic molecule with the simultaneous addition of a hydrogen atom to the resulting molecular fragments. Through the selective hydrogenolysis of glycerol in the presence of metallic catalysts and hydrogen, 1,2-propanediol (1,2-PD), 1,3-propanediol (1,3-PD), and ethylene glycol (EG) could be obtained [5]. Therefore, catalytic hydrogenolysis of glycerol is another alternative route to increase the profitability of biodiesel production plants as the products of glycerol hydrogenolysis can easily replace the chemical compounds, which at present are industrially produced mainly by using non-renewable sources. Propanediol, i.e., 1,2-PD, a three-carbon diol with a stereogenic center at the central carbon atom, is an important medium-value commodity chemical with a 4 % annual growth in the market size. It is used for polyester resins, liquid detergents, pharmaceuticals, cosmetics, tobacco humectants, flavors and fragrances, personal care, paints, animal feed, antifreeze, etc.

✉ Komandur V. R. Chary
kvrchary@iict.res.in

[1] Catalysis Division, Indian Institute of Chemical Technology, Hyderabad 500 007, India

[2] Nanomac Centre at Australian Institute for Bioengineering and Nanotechnology and School of Engineering, The University of Queensland, St. Lucia, QLD 4072, Australia

[3] School of Applied Sciences, RMIT University, GPO Box 2476V, Melbourne, VIC 3001, Australia

[6]. Traditionally, it is produced by the hydration of propylene oxide derived from propylene by either the chlorohydrin process or the hydroperoxide process. There has been a rapid expansion of the market for 1,2-PD as an antifreeze and de-icing agent because of the growing concern over the toxicity of ethylene glycol-based products to humans and animals. 1,3-PD is also another product obtained during glycerol hydrogenolysis, which is a high-value specialty chemical that is mainly used in specialty polyester fibers, films, and coatings. 1,3-PD is copolymerized with terephthalic acid to produce the polyester SORONA1 from DuPont, or CORTERRA1 from Shell, which has unique properties in terms of chemical resistance, light stability, elastic recovery, and dyeability [7, 8]. 1,3-PD is currently catalytically produced [9]. The production of these chemicals from bio-renewable glycerol can be both environmentally and economically attractive.

The glycerol hydrogenolysis reaction is suggested to proceed via dehydration of glycerol to acetol and 3-hydroxypropanal by acid catalysis and subsequent hydrogenation to the glycols by metal catalysts [6–9]. Besides the hydrogenolysis reaction, degradation reactions involving C–C breaking also occur. The products from C–C cracking are mainly ethylene glycol, methanol, ethanol and methane. Therefore, the selective conversion of glycerol to propanediols requires a suitable catalyst with acid sites/metal surface, favoring the cleavage of the glycerol C–O bonds (dehydration/hydrogenation) by hydrogen. Many supported metal catalysts have been reported for this type of reaction in liquid phase. Tomishige and co-workers [6–9] reported the use of supported group VIII metals (especially Ru/C and Rh/SiO_2) catalysts in combination with a strong solid acid (Amberlyst 15, 70) at mild temperatures of 120. 8 °C and H_2 pressures of 4–8 MPa. Chary et al. have demonstrated the vapor phase hydrogenolysis of glycerol reaction by using Ru-supported catalysts on supports like SBA-15 [12], MCM-41 [13], TiO_2 [14]. Feng et al. [15] investigated the effect of various supports (Al_2O_3, TiO_2, and ZrO_2) on Cu/ZnO/MOx catalysts and found that the support material can influence the metal particle size and the reaction routes, with TiO_2 and Al_2O_3 yielding the most selective catalysts for propanediols production in the vapor phase glycerol hydrogenolysis reaction. Vasiliadou et al. [16] investigated the Ru-based (γ-Al_2O_3, SiO_2, ZrO_2) catalysts were prepared by different precursors and found that among the tested catalysts, Ru catalyst prepared with the chloride precursor exhibited the highest activity towards glycerol hydrogenolysis.

In many instances, the active Ru is supported on oxides such as Al_2O_3, SiO_2, ZrO_2, and TiO_2 in combination with Zn or other transition metals such as Cu and Fe. The disadvantages of these supports are their low surface areas, high surface acidities, low activities, and phase transitions at higher temperatures, which make them unsuitable for industrial applications. The use of mixed oxide support or stabilization of these supports can overcome these problems [10]. The choice of a suitable Ru precursor and optimized activation conditions also allows the controlled preparation of small ruthenium particles on mixed oxide support to yield better results on glycerol hydrogenolysis on vapor phase reactions. To the best of our knowledge, development of supported Ru on mixed oxide materials for vapor phase hydrogenolysis of glycerol in aqueous medium has not been reported elsewhere.

In the recent past, the mixed oxide supports have been synthesized by co-precipitation, and sol–gel methods and explored for a number of catalytic processes. The correlation between catalytic activity and acid–base properties of TiO_2–ZrO_2 [11–14] has been investigated extensively. The TiO_2–ZrO_2 mixed oxide seems to be an interesting support material for ruthenium and is employed for vapor phase hydrogenolysis of glycerol.

In the present investigation, we report the catalytic behavior of Ru/TiO_2–ZrO_2 catalysts for the vapor phase hydrogenolysis of glycerol. The catalysts were also characterized by BET surface area, XRD, TPR, NH_3-TPD, TEM, XPS and CO chemisorption method. The aim of this research is to use the mixed oxide TiO_2–ZrO_2 as a support material in order to improve the conversion and selectivity of glycerol hydrogenolysis to 1,2-propanediol and 1,3-propanediol under mild reaction conditions. The effect of various loadings over Ru/TiO_2-ZrO_2 catalysts such as reaction time and recyclability were investigated to find out the optimum reaction conditions.

Experimental

Catalyst preparation

The TiO_2–ZrO_2 mixed oxide (1:1 wt%) support was prepared by the co-precipitation method. The requisite quantities of titanium isopropoxide in 2-propanol, zirconium(IV) propoxide in propanol, and NH_3 (40 % aqueous solution) were continuously stirred for 6 h at 70 °C. The precipitation was completed after 4–5 h of stirring at which the pH of the solution was 9. The precipitate thus obtained was then filtered, washed several times with deionized water until it was free from the base, dried overnight at 120 °C, and finally calcined at 500 °C for 6 h. The TiO_2–ZrO_2 support (Brunauer–Emmett–Teller (BET) surface area 170 m^2/g) is used for the preparation of supported ruthenium catalysts with varying Ru loadings from 1 to 6 wt% by deposition–precipitation method using an aqueous solution containing $RuCl_3 \cdot nH_2O$ (Aldrich) as precursor. In the DP method, the support was suspended in

an aqueous solution of 20–30 mL of de-ionized water and $RuCl_3 \cdot nH_2O$; $Ru(OH)_3$ was exclusively precipitated at 40 °C on the support by the slow addition of 1 M Na_2CO_3 solution until the pH of the solution was reached to 10.5. The resultant solid was filtered and washed with deionized water several times until no chloride ion was detected in the filtrate. The solid thus obtained was oven dried at 120 °C for 12 h. Prior to the catalyst characterization the catalysts are reduced under pure H_2 flow (50 mL/min) at 573 K for 3 h.

Catalyst characterization

X-ray diffraction patterns was obtained on Rigaku miniflex diffractometer using graphite filtered Cu Kα ($K = 0.15406$ nm) radiation. Determination of the ruthenium phase was made with the help of JCPDS data files.

The surface area, pore size distribution studies of the prereduced catalysts was estimated using N_2 adsorption isotherms at 77 K by the multipoint BET method taking 0.0162 nm^2 as its cross-sectional area using Autosorb 1 (Quantachrome instruments, USA).

The morphological analysis was carried out using transmission electron microscopy (TEM on a JEOL 100S microscope at high resolution (HR) on a JEOL 2010 microscope). Samples for both TEM analyses were prepared by adding 1 mg of reduced sample to 5 ml of methanol followed by sonication for 10 min. A few drops of suspension were placed on a hollow copper grid coated with a carbon film made in the laboratory.

Temperature-programmed reduction (TPR) experiments were carried out on AutoChem 2910 (Micromeritics, USA) instrument. In a typical experiment ca. 100 mg of oven dried $Ru/TiO_2–ZrO_2$ sample (dried at 110 °C for 12 h) was taken in a U-shaped quartz sample tube. Prior to TPR studies the catalyst sample was pretreated in an inert gas (Argon, 50 mL/min) at 200 °C. After pretreatment, the sample was cooled to ambient temperature and the carrier gas consisting of 5 % hydrogen balance argon (50 mL/min) was allowed to pass over the sample raising the temperature from ambient to 700 °C heating at the rate of 10 °C/min. The vapors produced during the reduction were condensed in a cold trap immersed in liquid nitrogen and isopropanol slurry. The hydrogen concentration in the effluent stream was monitored with the TCD and the areas under the peaks were integrated using GRAMS/32 software.

NH_3-TPD experiments were also conducted on the AutoChem 2910 instrument. Prior to TPD analysis the sample was pretreated by passage high purity (99.999 %) helium (50 mL/min) at 300 °C for 1 h. After pretreatment, the sample was saturated with 10 % NH_3 balance He mixture (75 mL/min) at 80 °C for 1 h and subsequently flushed at 105 °C for 2 h to remove physisorbed ammonia. TPD analysis was carried out from ambient temperature to 750 °C at a heating rate 10 °C/min. The amount of NH_3 desorbed was calculated using GRAMS/32 software.

X-ray photoelectron spectroscopy was used to study the chemical composition and oxidation state of catalyst surfaces. The XPS spectra of the catalysts were measured on a XPS spectrometer (Kratos-Axis 165) with Mg Kα radiation (hλ) 1253.6 eV) at 75 W. The Ru 3d and 3p core-level spectra were recorded and the corresponding binding energies were referenced to the C 1 s line at 284.6 eV (accuracy within (0.2 eV)). The background pressure during the data acquisition was kept below 10^{-10} bar.

CO chemisorption measurements were carried out on AutoChem 2910 (Micromeritics, USA) instrument. Prior to adsorption measurements, ca. 100 mg of the sample was reduced in a flow of hydrogen (50 mL/min) at 300 °C for 3 h and flushed out subsequently in a pure helium gas flow for an hour at 300 °C. The sample was subsequently cooled to ambient temperature in the same He stream. CO uptake was determined by injecting pulses of 9.96 % CO balanced helium from a calibrated on-line sampling valve into the helium stream passing over the reduced samples at 300 °C. Ruthenium surface area, percentage dispersion and Ru average particle size were calculated assuming the stoichiometric factor (CO/Ru) as 1. Adsorption was deemed to be complete after three successive runs showed similar peak areas.

Catalytic activity

Hydrogenolysis of glycerol (>99 % MERCK Chemicals) was carried out over the catalysts in a vertical down-flow glass reactor at 230 °C and operating under normal atmospheric pressure. In the typical reaction ca. 500 mg of the catalyst, diluted with double the amount of quartz grains was packed between the layers of quartz wool. The upper portion of the reactor was filled with glass beads, which served as pre-heater for the reactants. Prior to the reaction, the catalyst was reduced in a flow of hydrogen (100 mL/min) at 300 °C for 3 h. After reduction the reactor was fed with glycerol at 230 °C. Hydrogen and an aqueous solution of glycerol were introduced into the reactor through a heated evaporator. The liquid products were collected in a condenser to be analyzed every 60 min by GC fed. The reaction products were analyzed by Shimadzu-GC 2014 gas chromatograph equipped with a carbowax capillary column with a flame-ionization detector (FID). The products were also identified using HP-5973 quadrupole GC-MSD system using carbowax capillary column.

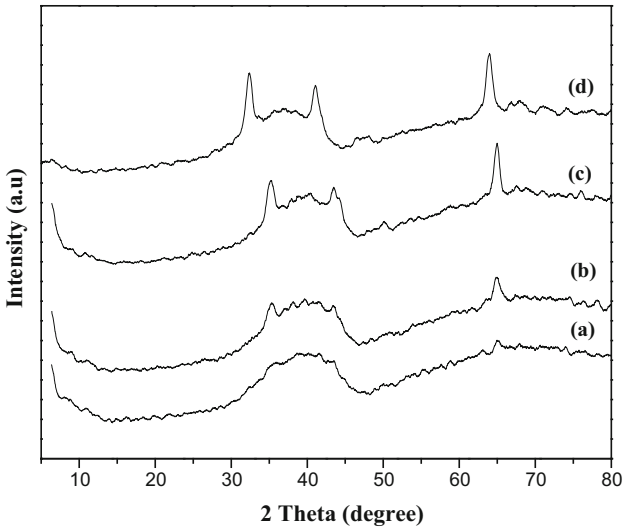

Fig. 1 XRD profiles of various $Ru/TiO_2–ZrO_2$ Catalysts (*a*) $1Ru/TiO_2–ZrO_2$, (*b*) $3Ru/TiO_2–ZrO_2$, (*c*) $5Ru/TiO_2–ZrO_2$, (*d*) $6Ru/TiO_2–ZrO_2$

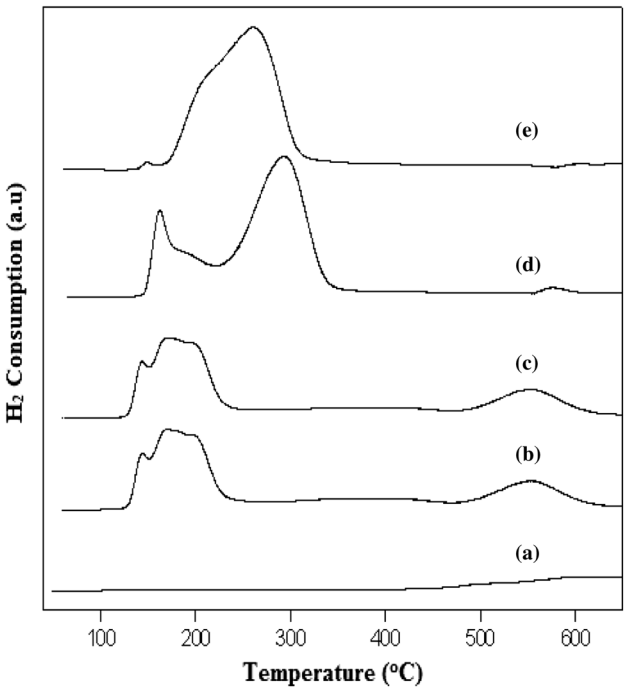

Fig. 2 H_2 TPR profiles of various $Ru/TiO_2–ZrO_2$ catalysts (*a*) $1Ru/TiO_2–ZrO_2$, (*b*) $3Ru/TiO_2–ZrO_2$, (*c*) $5Ru/TiO_2–ZrO_2$, (*d*) $6Ru/TiO_2–ZrO_2$

Results and discussion

Characterization of Ru deposited on $TiO_2–ZrO_2$

The X-ray diffraction patterns of various Ru catalysts supported on $TiO_2–ZrO_2$ are shown in Fig. 1. As can be seen from Fig. 1, ruthenium supported on $TiO_2–ZrO_2$ did not show any reflections due to ZrO_2 or TiO_2 (1:1) catalysts, which confirms that the $TiO_2–ZrO_2$ phase is an amorphous or poorly crystalline material [10]. It is also observed that 1, 3 wt% $Ru/TiO_2–ZrO_2$ samples show a reflection at around the 2θ range of 34°, 44° due to the amorphous ruthenium [4]. This peak becomes sharp from $5Ru/TiO_2–ZrO_2$ and gives a clear reflection at $6Ru/TiO_2–ZrO_2$ indicating the crystallization of ruthenium beyond $5Ru/TiO_2–ZrO_2$. This indicates the formation of Ru^0 phase [14]. Another sharp reflection at 2θ range of 65° represents the ruthenium combined with the mixed oxide phase of $TiO_2–ZrO_2$ support [17].

Temperature-programmed reduction profiles of various $Ru/TiO_2–ZrO_2$ are shown in Fig. 2 and the hydrogen consumption during TPR are reported in Table 1. The TPR profiles reveal that the catalysts exhibited main reduction peak at 147–260 °C related to reduction of Ru^{3+}/Ru^0. These peaks are broad possibly due to location of ruthenium ions in different environments. But at low ruthenium loading 1–3 wt% the signal was split in two (α,β) and these peaks are with in the range of first T_{max} of the other samples. The first peak in TPR of these low loading samples (1–3 wt% Ru) is due to unsupported ruthenium chloride and the second one is due to reduction of supported ruthenium chloride. The high temperature peak around 550 °C is attributed to Ru strongly interacting with the support. The T_{max} of the main reduction peak tend to increase with ruthenium loading indicating the crystallization of ruthenium particles, i.e., larger particles tend to reduce at slightly higher temperature [4].

The ammonia TPD profiles of the various $Ru/TiO_2–ZrO_2$ catalysts are presented in Fig. 3. Temperature-programmed desorption of ammonia was performed on all the catalysts to obtain the information about differences in the surface structure of the catalyst. The ammonia uptake values and the T_{max} values are given in Table 2. In the present study ammonia TPD method was adopted to study the acidity of $Ru/TiO_2–ZrO_2$ catalysts. As can be seen from Fig. 3 that the acidic sites are distributed in maximum three T_{max} regions, one due to low acid strength (low T_{max} region), one due to moderate acid strength (medium T_{max} region) and other is due to strong acid strength (high T_{max} region). $3Ru/TiO_2–ZrO_2$ exhibit more number of acidic sites confined to weak and strong acid strength. In case of catalysts $5Ru/TiO_2–ZrO_2$ and $6Ru/TiO_2–ZrO_2$, moderate and strong acid sites are found to increase with the increase of ruthenium loading. It is interesting to note that the acidity values of $3Ru/TiO_2–ZrO_2–6Ru/TiO_2–ZrO_2$ are decreasing due to increase in Ru-metal percentage on acidic titania–zirconia support [18–24].

The catalysts $Ru/TiO_2–ZrO_2$ (Fig. 4) show the presence of metal particles on external surface of the support. The

Table 1 Results of temperature-programmed reduction of various $Ru/TiO_2–ZrO_2$ catalysts

Ru wt%	Tmax[1] (°C)	H_2 uptake (μmol/g)	Tmax[2] (°C)	H_2 uptake (μmol/g)	Tmax[3] (°C)	H_2 uptake (μmol/g) (°C)	Total H_2 uptake (μmol/g)
1.0	147	12	278	47	536	61	120
2.0	163	16	270	123	514	24	163
5.0	162	57	292	507	570	17	581
6.0	161	2	261	822	–	–	824

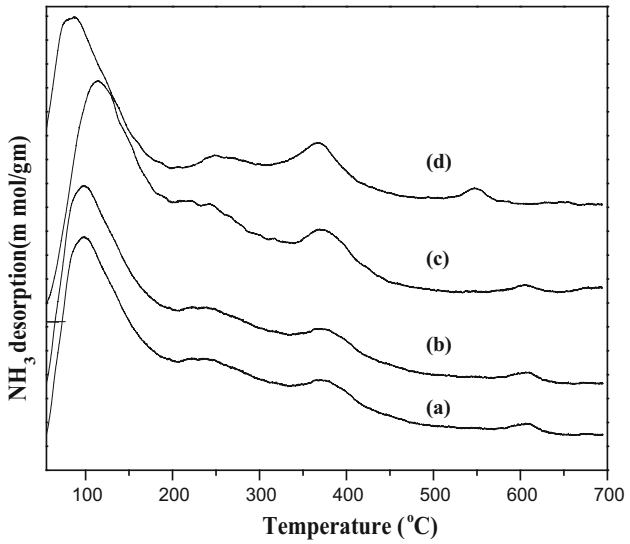

Fig. 3 NH_3-TPD profiles of various $Ru/TiO_2–ZrO_2$ catalysts (*a*) $1Ru/TiO_2–ZrO_2$, (*b*) $3Ru/TiO_2–ZrO_2$, (*c*) $5Ru/TiO_2–ZrO_2$, (*d*) $6Ru/TiO_2–ZrO_2$

Table 2 Temperature-programmed desorption results of NH_3 of various $Ru/TiO_2–ZrO_2$ catalysts

Ru loading (wt%)	NH_3 uptake (μmol/g)			Total NH_3 uptake (μmol/g)
	Weak	Medium	Strong	
1.0	200	20	15	235
3.0	210	37	22	269
5.0	125	54	25	204
6.0	90	70	37	197

particle sizes of the $Ru/TiO_2–ZrO_2$ catalysts were estimated from TEM and CO chemisorption. The TEM images of $1Ru/TiO_2–ZrO_2$ and $3Ru/TiO_2–ZrO_2$ catalysts reveal the presence of highly dispersed Ru particles confined to $TiO_2–ZrO_2$ support oxide which is not the same in $6Ru/TiO_2–ZrO_2$. The average particle size of ruthenium particles estimated from CO chemisorption is in good agreement with that of estimated from the TEM results.

The nature of surface species of the $Ru/TiO_2–ZrO_2$ catalysts was investigated by the XPS technique. Figure 5a–c show Ti 2p, Zr 3d and Ru 3p XPS of various $Ru/TiO_2–ZrO_2$ catalysts. Figure 5a show the binding energies of Ti 2p photoelectron peaks at 458.5 and 464.4 eV for Ti $2p_{3/2}$ and Ti $2p_{1/2}$ lines, respectively, and these are in agreement with the values reported in the literature [19, 25, 26]. Figure 5b show the Zr $3d_{5/2}$ and Zr $3d_{3/2}$ binding energy values in the range of 182.3 and 184.7 eV, respectively, which is in agreement with the values reported in the literature [25]. The binding energies of Zr $3d_{5/2}$ and its full width at half-maximum (FWHM) values are reported in Table 3. The constant FWHM values are found to be around 1.6, implying that only one type of doublet is present in the XPS spectrum. This provides an evidence for the presence of a single type of zirconium oxide with an oxidation state of 4+. The intensities of the Zr 3d core-level spectra do not change much with increase in ruthenium loading.

The binding energy values of Zr 3d and Ti 2p did not changed much with varying ruthenium loadings, indicating the integrity of the support structure, which was not modified by ruthenium deposition. The binding energies of Ti $2p_{3/2}$ and its FWHM values are reported in Table 3. The constant binding energies of Ti $2p_{3/2}$ and its FWHM values indicate the presence of one type of titanium oxide with an oxidation state of 4+. Figure 5c represents the XPS of various ruthenium supported $TiO_2–ZrO_2$ catalysts for Ru $3p_{5/2}$ and Ru $3p_{3/2}$ indicating the electronic state and environment of Ru^0 species present in supported catalysts. The binding energies and their FWHM values are reported in Table 3. Generally Ru^0 possess the binding energy values 463.0–462.5 eV [26]. The BE values for Ru $3p_{5/2}$ (484.0–484.5 eV) and Ru $3p_{3/2}$ (463.5–462.5 eV) in supported ruthenium catalysts are significantly higher than that of Ru^0 (Fig. 5). Generally, this phenomenon can be understood as the strong metal–support interaction (SMSI) effect.

With increase in ruthenium loading the binding energy of Ru $3p_{5/2}$ and Ru $3p_{3/2}$ shifted towards lower side up to 3 wt% and remains constant at higher Ru loadings. Since smaller ruthenium particles have higher binding energy and larger particles have lower binding energy [26]. This might be due to interaction of small ruthenium particles strongly

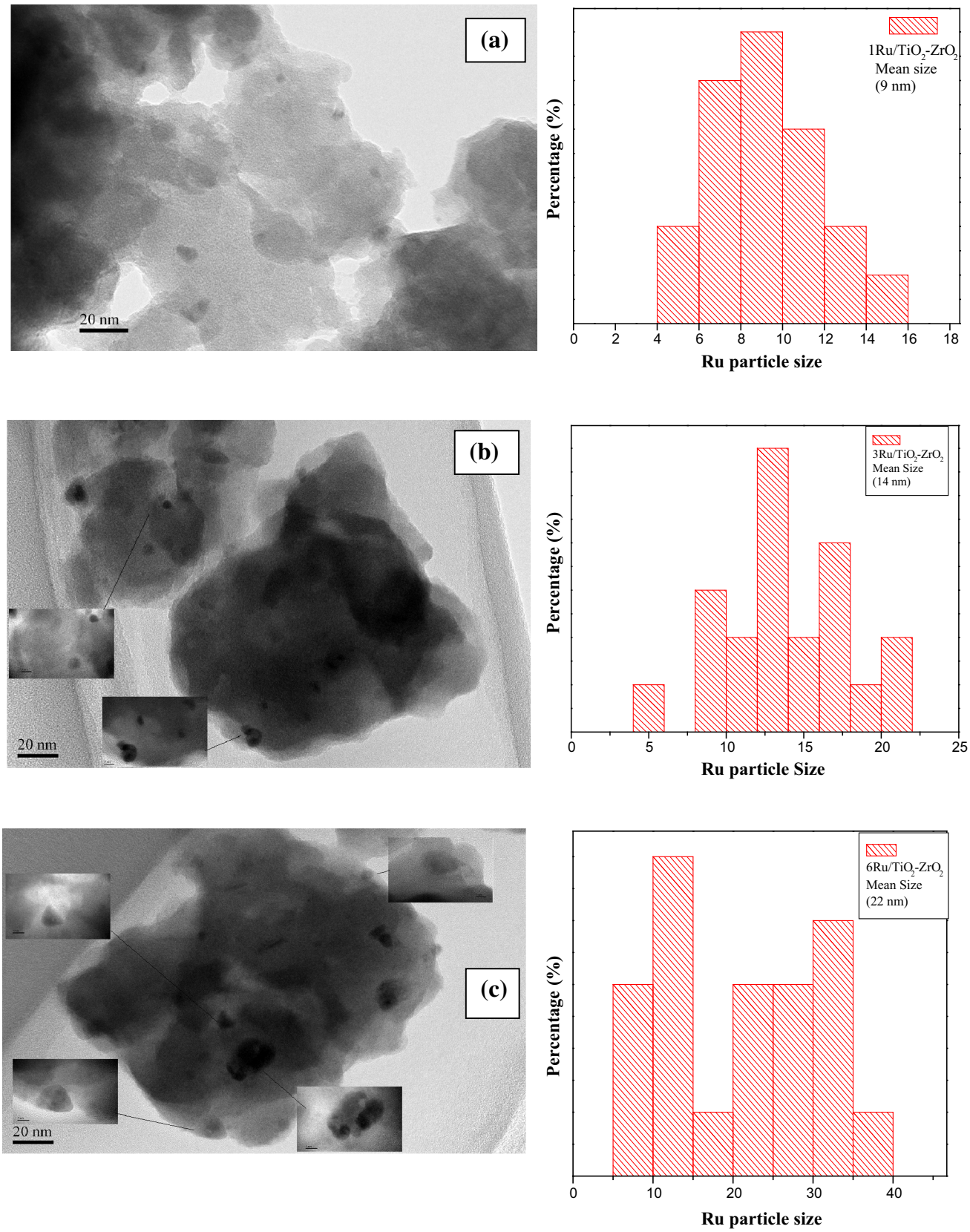

Fig. 4 TEM images of various $Ru/TiO_2–ZrO_2$ catalysts (*a*) $1Ru/TiO_2–ZrO_2$, (*b*) $3Ru/TiO_2–ZrO_2$, (*c*) $6Ru/TiO_2–ZrO_2$

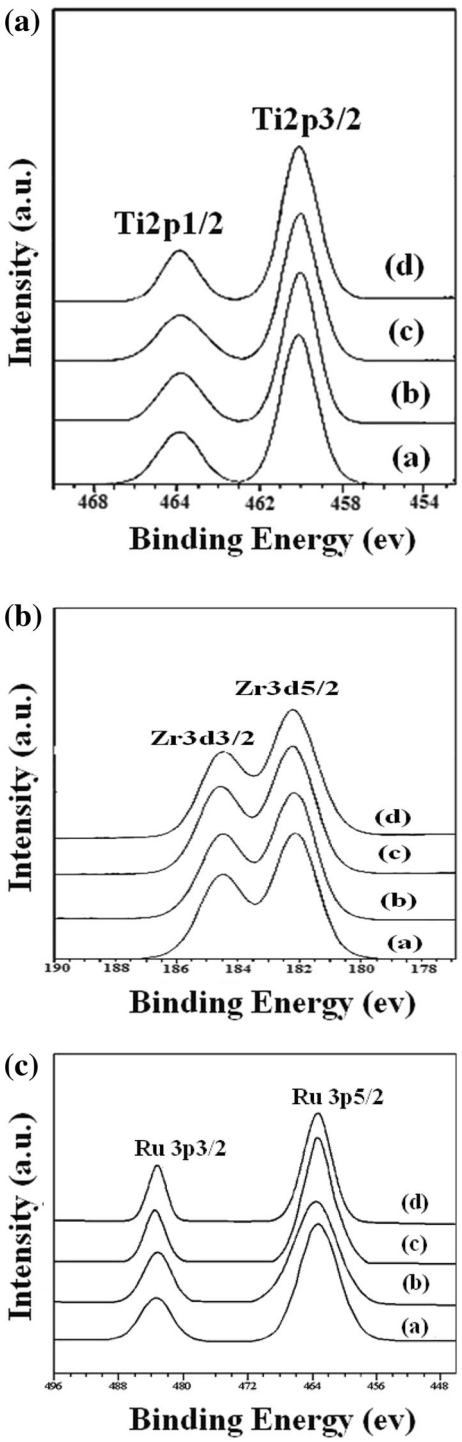

Fig. 5 **a** Ti 2p XPS spectra of various $Ru/TiO_2–ZrO_2$ catalysts **a** $1Ru/TiO_2–ZrO_2$, **b** $3Ru/TiO_2–ZrO_2$, **c** $5Ru/TiO_2–ZrO_2$, **d** $6Ru/TiO_2$-ZrO_2 . **b** Zr 3d XPS spectra of various $Ru/TiO_2–ZrO_2$ catalysts **a** $1Ru/TiO_2–ZrO_2$, **b** $3Ru/TiO_2–ZrO_2$, **c** $5Ru/TiO_2–ZrO_2$, **d** $6Ru/TiO–ZrO_2$.**c** Ru 3p XPS spectra of various $Ru/TiO_2–ZrO_2$ catalysts **a**$1Ru/TiO_2–ZrO_2$, **b** $3Ru/TiO_2–ZrO_2$, **c** $5Ru/TiO_2–ZrO_2$, **d** $6Ru/TiO_2–ZrO_2$

with the support. These results clearly suggest that with increase of Ru loading the metal–support interaction decreases and the dispersion also decreases. The XPS intensity ratios of Ru $3p_{5/2}$/Zr $3d_{5/2}$ for various Ru/TiO_2-ZrO_2 catalysts are reported in Table 3. The intensity ratio increases with increasing of ruthenium loading up to 3 wt% and did not change appreciably with further increase in Ru loading. These results suggest that number of active Ru sites increase up to 3 wt% with increasing Ru loading and no significant effect at higher loadings is noticed due to the formation of large agglomeration of Ru^0 crystallites. Thus, a low dispersion of ruthenium is noticed at higher loadings by CO chemisorption method. The present XPS results are in well agreement with the dispersion of ruthenium determined by XRD and CO chemisorption method.

The BET surface area of pure Titania–Zirconia is 170.0 m^2/g. The surface area (Table 4) tends to decrease with the increase of ruthenium loading on Titania–Zirconia mixed oxide support. The particle size of ruthenium also increases smoothly up to 3 wt% and tends to increase exponentially from 5 to 6 wt%. The increase in the crystallite size beyond 5 wt% indicates that the overloading of the metal lead to increase in the crystallite size due to agglomeration of ruthenium particles.

The physical properties of catalysts such as dispersion, metal surface area and average particle size obtained from CO chemisorption are given in Table 4. Assuming the particle to be cubic with five sides exposed to the gas plane is the dispersion of Ru was calculated from CO chemisorption using the following equation:

$$\% \text{ Dispersion} = \frac{(\text{Number of surface ruthenium atoms} \times 100)}{\text{Total number of ruthenium atoms}}$$

$$\text{Average particle size (nm)} = \frac{6000}{(\text{Ru metal area per gram of Ru} \times \text{Ru density})}$$

The ruthenium metal areas were determined using the equation $S_{CO} = n^S_m X_m n_s^{-1}$, where S_{CO} is the total metallic surface area, n^S_m is the CO consumption and X_m is chemisorption stoichiometry at monolayer coverage, and n_s^{-1} is the number of ruthenium atoms per unit surface area. It can be observed from the Table 4 that the dispersion of ruthenium and metal area of the catalyst decreases with increase of the ruthenium loading on $TiO_2–ZrO_2$ support. However, the particle size of ruthenium increases linearly up to 3 wt% and tend to increase exponentially at higher loading. The metal area per gram of ruthenium and number of active sites available per gram of the catalyst tend to increase up to 3 wt% and tends to decrease slightly from 5 wt% loading. The decrease in metal area and the number of available active sites at higher loadings in $6Ru/TiO_2–ZrO_2$ is due to overloading of the catalysts which lead to agglomeration of ruthenium particles to larger particles, which is in good agreement with TEM and XRD results.

Table 3 Binding energies (eV), FWHM, XPS atomic ratios of Zr $3d_{5/2}$, Ti $2p_{3/2}$ and Ru $3p_{3/2}$ for $Ru/TiO_2–ZrO_2$ catalysts

Ru wt%	Position and FWHM of Zr $3d_{5/2}$	Position and FWHM of Ti $2p_{3/2}$	Position and FWHM of Ru $2p_{3/2}$	XPS intensity Ru 3p/Zr 3d	XPS intensity Ru 3p/Ti 2p
1.0	182.1 (1.5)	458.1 (2.0)	462.5(2.7)	0.06	1.3
3.0	182.2 (1.6)	458.1 (1.9)	462.4(2.6)	0.11	1.4
5.0	182.3 (1.6)	458.3 (2.0)	461.4(2.5)	0.15	1.6
6.0	182.2 (1.7)	458.1 (2.0)	461.2(2.4)	0.18	1.6

Table 4 BET surface area and CO chemisorption of various Ruthenium on Titania–Zirconia catalysts

Catalyst	BET surface area $(m^2/g)^a$	Dispersion (%)	Metal surface area $(m^2/g)_{Ru}$	Particle size $(nm)^b$	Particle size $(nm)^c$
$TiO_2–ZrO_2$	170.0	–	–	–	–
$1Ru/TiO_2–ZrO_2$	159.0	34.0	6.0	7.0	9.0
$3Ru/TiO_2–ZrO_2$	147.0	29.0	5.0	11.0	14.0
$5Ru/TiO_2–ZrO_2$	99.0	21.0	3.0	27.0	19.0
$6Ru/TiO_2–ZrO_2$	67.0	8.0	1.0	26.0	22.0

The same can be observed from the CO uptake values, which increased up to at higher loading catalyst $6Ru/TiO_2–ZrO_2$.

The catalytic performance of $TiO_2–ZrO_2$ supported Ru catalysts in the vapor phase glycerol hydrogenolysis reaction was carried out at 230 °C and at normal atmospheric pressure. The Fig. 6 shows the results of hydrogenolysis activity of various $Ru/TiO_2–ZrO_2$ catalysts. From the Fig. 6, it is clear that the hydrogenolysis activity increases up to 3 wt% and tends to decline at further ruthenium loadings. The hydrogenolysis activity expressed in terms of (%) conversion increased from 40 % for 1 wt% to 52 % for 3 wt% and tends to decrease slightly at further ruthenium loadings (Table 5). However, the selectivity as shown from the Fig. 6 represents 1,2-propanediol—35 %, 1,3-propanediol—15 %, 2-propanol—8 %, 1-propanol—14 % with 10 % of dehydration product hydroxyacetone, 9 % of ethylene glycol, 4 % ethanol and 5 % methanol are degradation products. Miyazawa et al. [27] used a combination of Ru/C together with the cation exchange resin amberlyst-15 as acid catalyst. They observed the formation of both 1,2-propanediol and 1,3-propanediol. It was suggested that glycerol is first dehydrated through an acid-catalyzed reaction to acetol or 3-hydroxypropionaldehyde and that the subsequent hydrogenation of the intermediates leads to 1,2-propanediol and 1,3-propanediol, respectively. A common feature of all these studies is the low selectivity to 1,3-propanediol. According to Schlaf et al. [28], acid-catalyzed hydrogenolytic cleavage of –OH group occurs through an initial protonation of the hydroxyl group that leads to the formation of a carbocation and water.

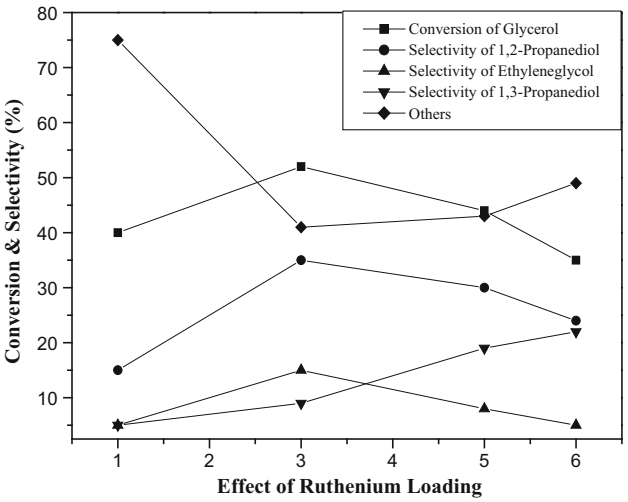

Fig. 6 Effect of metal loading of various $Ru/TiO_2–ZrO_2$ catalysts on conversion of glycerol hydrogenolysis reaction

Thermodynamically, the formation of a secondary carbocation is more favored than the formation of a primary carbocation. Therefore, operating under acid conditions should bring about higher selectivity to 1,3-propanediol. The fact that product distribution is usually shifted towards 1,2-propanediol seems to be a complex function of operating conditions, catalyst and starting materials. Another factor that must be taken into account in propanediols formation is the higher stability of the intermediate acetol compared to 3-hydroxypropionaldehyde, which is readily hydrogenated to 1,3-propanediol or dehydrated to acrolein

[29]. These better conversions/selectivities exhibited by lower Ru loading catalysts viz., 1Ru/TiO_2–ZrO_2 and 3Ru/TiO_2–ZrO_2 are also due to the formation of nano Ru particles, acidic support and high dispersion as evidenced from the findings of BET surface area, CO chemisorption and TPR measurements. The catalytic activity exhibited by various Ru/TiO_2–ZrO_2 catalysts was found to be superior in vapor phase hydrogenolysis reaction at low hydrogen flow rates [140 mL/min] at normal atmospheric pressure. In the case of 6Ru/TiO_2-ZrO_2 catalyst conversion (35 %) and selectivity (1,2-PD-24 %, 1,3-PD-5 %, 1-Propanol-7 % and Ethylene glycol-22 %) has decreased due to the formation of ruthenium particles as crystallites which are evidenced from XRD, TEM, TPR and CO chemisorption data. Martin et al. [30] studied Ru and Pt catalysts on batch run glycerol hydrogenolysis reaction and observed Ru catalyst showed better activity and stability compared to Pt catalysts. Therefore, the superior activity of Ru/TiO_2–ZrO_2 is probably due to higher dispersion of Ru on TiO_2–ZrO_2 than Ru on other supports and also due to strong metal–support interaction between Ru with TiO_2–ZrO_2 support. Tomishige et al. [31] proposed the reaction mechanism for glycerol hydrogenolysis in liquid phase on various Ru catalysts [12] with better conversion and selectivities. The activity of the catalysts at lower loadings (1–3 Ru/TiO_2–ZrO_2) is rather high due to their strong interaction with TiO_2-ZrO_2 as seen from the TPR patterns showing the presence of ruthenium active sites for the formation of desired hydrogenolysis products of glycerol reaction. Thus, the findings of BET, CO chemisorption further support the catalytic properties exhibited by various Ru/TiO_2–ZrO_2 catalysts during glycerol hydrogenolysis reaction. However, the TPR patterns also reveal the formation of bulk ruthenium leading to sharp reduction peaks for 6.0 wt% Ru catalysts.

Effect of ruthenium loading

Catalytic activity tests with the bare supports under the similar conditions used in this study resulted in very low conversion (<10 %), also the initial rates of conversion of glycerol and formation of propanediol have a proportional increase with the catalyst amount. However, as the reaction time increases, the excess catalyst further promotes excessive hydrogenolysis reaction converting glycerol to propanediols. Hence, to obtain a good conversion of glycerol with high selectivity to propanediols an optimal amount of catalyst active sites [31, 32] should be available depending on the reaction time. From Fig. 6 it can be inferred that the conversion of glycerol increases with Ru loading up to 3 wt% and decreases slightly at higher Ru loadings. However, the selectivity towards 1,2-propanediol, 1,3-propanediol increased up to 3 wt% and decreases slightly beyond this loading. This is probably due to the presence of strong and weak acid sites which favors the formation of 1,2-propanediol and 1,3-propanediol, respectively [33, 34]. Feng et al. also reported similar findings [13]. The decrease of glycerol conversion at higher Ru loadings is probably due to weak metal–support interaction between ruthenium and support as evidenced from TPR and CO chemisorption measurements [35, 36]. The catalytic behavior of various Ru catalysts with varying parameters discussed in terms of the findings of surface characterization techniques.

Dependence of catalytic properties on reaction time

The time on stream studies on the 1–6 wt% Ru/TiO_2-ZrO_2 catalysts were investigated to understand the stability of catalysts during glycerol hydrogenolysis and the results are shown in Fig. 7. These results show that 3Ru/TiO_2–ZrO_2 exhibit higher conversion (52 %) and showed stability compared to other catalysts. The catalysts prepared by DP method exhibited better conversions and good selectivities towards propanediols. The results suggest that 6Ru/TiO_2–ZrO_2 show lower conversion and selectivity than 3Ru/TiO_2–ZrO_2, due to their increased particle sizes. Although the initial activity is better for 6Ru/TiO_2–ZrO_2 catalysts, the activity abruptly dropped from 35 to 20 % within 7 h of operation. The 1Ru/TiO_2–ZrO_2 and 3Ru/TiO_2–ZrO_2 catalysts exhibit initial activity of 40 and 52 % but they decreased to 35 and 52 % with time compared to other

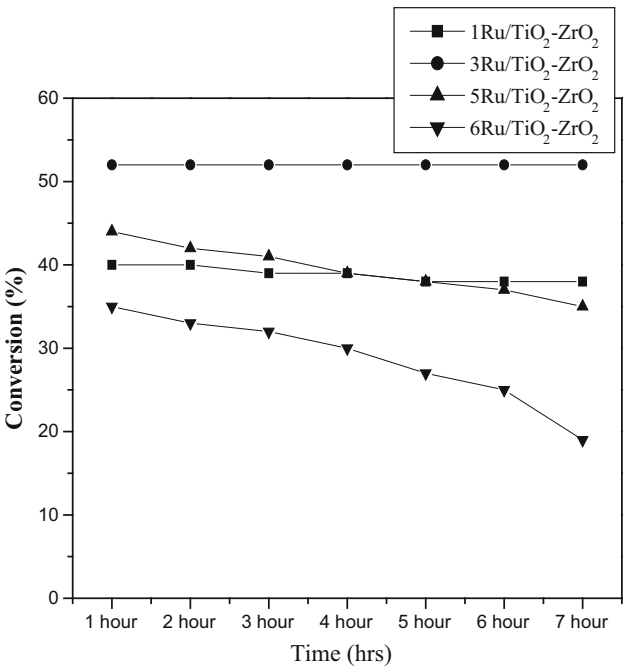

Fig. 7 Time on stream studies of various Ru/TiO_2–ZrO_2 catalysts on conversion of glycerol

catalysts, suggesting that 3Ru/TiO_2–ZrO_2 was a best catalyst for the vapor phase glycerol hydrogenolysis of our present investigation. The reasons for faster deactivation of catalyst 6Ru/TiO_2–ZrO_2 are probably due to carbon deposition and agglomerisation during the reaction. The catalytic activity is correlated with the crystallite size of Ru on different catalysts. The 6Ru/TiO_2–ZrO_2 catalyst is attributed to the decrease in the number of active sites of ruthenium on TiO_2–ZrO_2 due to agglomeration as evident from XRD, TPR and CO chemisorption results. The stability of the 3Ru/TiO_2–ZrO_2 catalyst during the hydrogenolysis of glycerol was investigated over 7 h time on stream at 230 °C and the results are showed in Fig. 7. In a time interval of 7 h, glycerol conversion decreased from 35 to 19 % for 6Ru/TiO_2–ZrO_2 catalyst. It can be seen from Fig. 7 that conversion of glycerol remains steady till 7 h for 3Ru/TiO_2–ZrO_2 catalyst. This decline in conversion might be due to the structural changes in the catalyst due to the deactivation of the catalyst leading to the agglomerisation of Ru active metal species.

Effect of temperature

Temperature has a significant effect on the overall yield of the propanediol. In the present work, the reactions were carried out at 230 and 280 °C and at hydrogen flow rate of 140 mL/min in the presence of best activity 3Ru/TiO_2-ZrO_2 catalyst. The effect of temperature on the conversion and selectivity of the reaction are shown in Fig. 8. As the temperature of the reaction increased from 230 to 280 °C, there is a marginal increase in the conversion of glycerol. However, the selectivity of 1,2-propanediol (23 %), 1,3-propanediol (4 %) and ethylene glycol (11 %), 2-P (5 %), 1-P (<5 %), ethyl alcohol (8 %) and methanol (13 %) also decreased considerably at reaction temperature 280 °C. Our present study suggests that at 230 °C, the hydrogenolysis of glycerol reaction provides optimum yields towards desired hydrogenolysis products. The reason for the increase in degradation products at higher temperatures is probably due to further hydrogenolysis of propanediols to yield lower alcohols [33, 34].

Effect of glycerol concentration

The effect of glycerol concentration or water content on glycerol hydrogenolysis was studied. The results presented in Fig. 9 clearly show a considerable decline in the glycerol conversion with increase in glycerol concentration. It is known that glycerol conversion and selectivity was higher at low glycerol concentration. The selectivities obtained towards 1,2-Propanediol (35 %), 1,3-Propanediol (15 %), EG(9 %), 2-propanol(8 %), 1-propanol (14 %), ethyl alcohol (4 %) and methanol (5 %) at lower glycerol

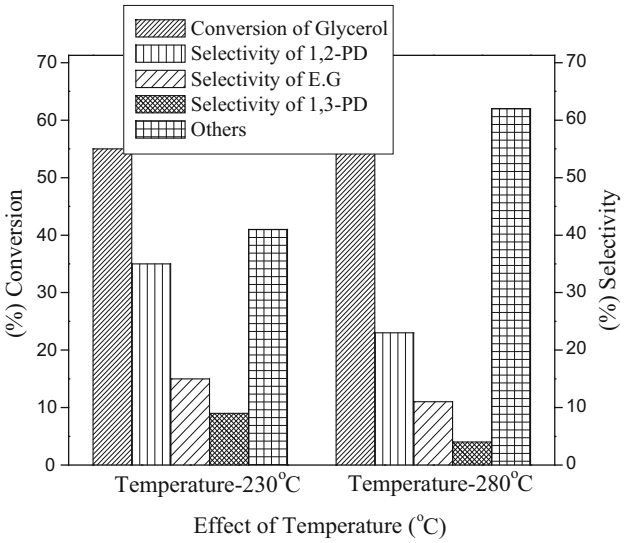

Fig. 8 Effect of Temperature of 3Ru/TiO_2–ZrO_2 catalyst on glycerol hydrogenolysis reaction. Reaction conditions: Catalyst weight: 0.5 g, 3Ru/TiO_2–ZrO_2, Temperature varied: 230 and 280 °C, Feed rate: 1 ml/h, H_2 flow rate: 140 mL/min, glycerol concentration: 20 wt%

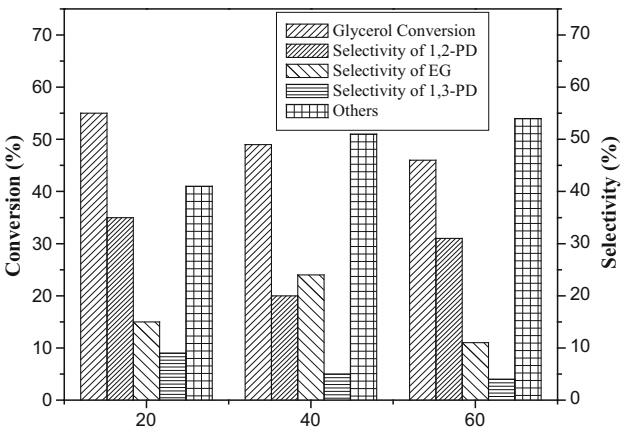

Fig. 9 Effect of Glycerol concentration of 3Ru/TiO_2-ZrO_2 catalyst on glycerol hydrogenolysis reaction Reaction conditions: Catalyst weight: 0.5 g 3Ru/TiO_2–ZrO_2, temperature: 230 °C, feed rate: 1 ml/h, H_2 flow rate: 140 mL/min; glycerol concentration: 20 and 60 wt%

concentration—20 wt% (WHSV-2.09 h^{-1}). The low conversion and selectivities at high glycerol concentration-40 wt% (WHSV-2.19 h^{-1}) for the respective products are 1,2-Propanediol (31 %), 1,3-Propanediol (4 %) and Ethylene glycol (8 %), 2-P (7 %), 1-P (<5 %), Ethyl alcohol (9 %) and Methanol (12 %) as expected, since the available number of Ru sites is constant [32].

Effect of H_2 flow rate

The role of H_2 flow rate hydrogenolysis was studied. The results presented in Fig. 10 clearly show a considerable decline in glycerol conversion with increase in glycerol

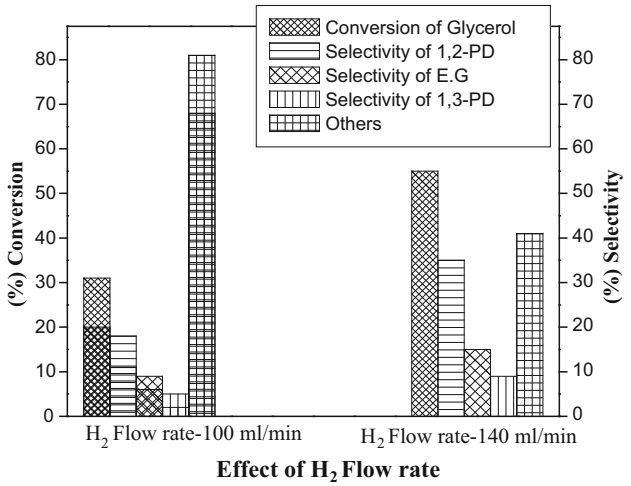

Fig. 10 Effect of H_2 flow rate on $3Ru/TiO_2–ZrO_2$ catalyst on glycerol hydrogenolysis reaction. Reaction conditions: catalyst weight: 0.5 g, $3Ru/TiO_2–ZrO_2$, temperature: 230 °C, feed rate: 1 ml/h, H_2 flow rate: 140 and 100 mL/min, glycerol concentration: 20 wt%

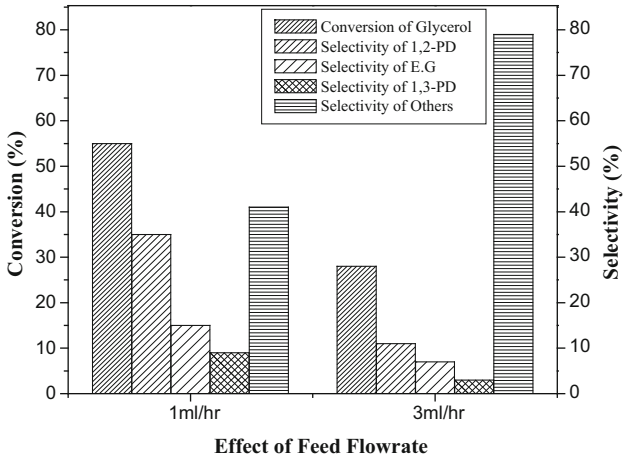

Fig. 11 Effect of feed flow rate on $3Ru/TiO_2–ZrO_2$ catalyst of glycerol hydrogenolysis reaction. Reaction conditions: Catalyst weight: 0.5 g, $3Ru/TiO_2–ZrO_2$: temperature: 230 °C, Feed rate: 1 and 3 ml/h, H_2 flow rate: 140 ml/min; Glycerol concentration: 20 wt%

concentration. It is known that glycerol conversion/selectivity was higher at low glycerol concentration. The selectivities obtained at H_2 flow rate 100 mL/min were 1,2-propanediol (18 %), 1,3-propanediol (8 %) and ethylene glycol (9 %), 2-P (7 %), 1-P (<8 %), Ethyl alcohol (10 %) and Methanol (13 %). The low conversion and selectivity at low H_2 flow rate (100 mL/min) is as expected, since the availability of hydrogen required for the hydrogenation of hydroxyacetone formed during the reaction is less [32].

Effect of feed flow rate

The influence of feed flow rate on glycerol hydrogenolysis was examined and the results are presented in Fig. 11. It shows that decrease in glycerol conversion was noticed with increase of glycerol flow rate from 1 mL/h (WHSV—2.09 h^{-1}) to 3 mL/hr (WHSV—6.27 h^{-1}). It is known that glycerol conversion is higher at low glycerol flow rate of 1 mL/h. The selectivities obtained for glycerol hydrogenolysis products at glycerol flow rate of 3 mL/h is 1,2-propanediol (11 %), 1,3-propanediol (3 %) and ethylene glycol (7 %), 2-P (6 %), 1-P (<5 %), Ethyl alcohol (6 %) and Methanol (10 %) at higher feed flow rate of glycerol. The low conversion and selectivities at high glycerol feed flow rate is as expected, since the available number of Ru sites remain unchanged [32].

Recyclability studies of catalyst $3Ru/TiO_2–ZrO_2$ and its structural aspects

The results of two successive reactions of best activity catalyst $3Ru/TiO_2–ZrO_2$ were summarized in Fig. 12.

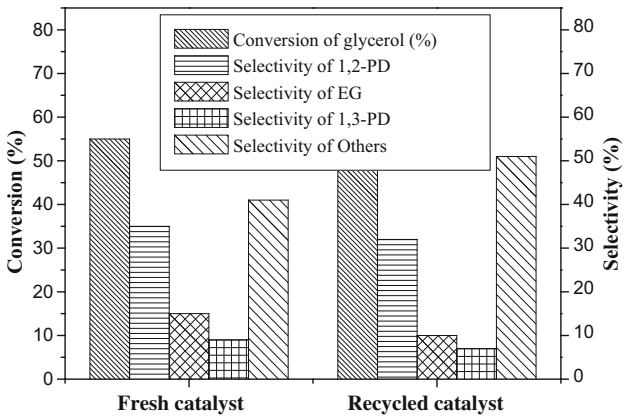

Fig. 12 Reusability studies of $3Ru/TiO_2–ZrO_2$ catalysts

After a typical run at 230 °C and at normal atmospheric pressure for 7 h, the recyclability of the catalyst was investigated. The hydrogenolysis of $3Ru/TiO_2–ZrO_2$ was carried out under relatively different conditions. There is a possibility of structural changes during the reaction and poisoning of the active metal sites. A simple switch off the coked $3Ru/TiO_2–ZrO_2$ catalysts to a flow of 20 vol% air flow and dried at the temperature (350 °C) was sufficient for a full regeneration of the deactivated $3Ru/TiO_2–ZrO_2$ catalyst shown in Fig. 8. Another reaction was carried out using the recycled catalyst, fresh glycerol feed under the same conditions. The recovered $3Ru/TiO_2–ZrO_2$ catalyst was found to be very active in the repeated run. Moreover, the conversion of glycerol increased marginally in the repeated reaction. The selectivity also remained increased slightly for all the retested catalysts. This suggested that a

Table 5 Effect of ruthenium loading on conversion/selectivity for hydrogenolysis of glycerol

Ru Wt (%)	Conversion (%)	Selectivity (%)						
		1,2-Propanediol	1,3-Propanediol	Hydroxy-acetone	1-Propanol	2-Propanol	Ethylene glycol	Others
TiO_2–ZrO_2	10	–	–	50	–	–	–	50
1Ru/TiO_2–ZrO_2	40	15	5	35	11	6	5	23
3Ru/TiO_2–ZrO_2	52	35	15	10	14	8	9	09
5Ru/TiO_2–ZrO_2	44	30	8	5	10	5	19	23
6Ru/TiO_2–ZrO_2	35	24	5	–	7	–	22	42

[a] Calculated from N_2 physisorption method

[b] Calculated from CO chemisorption method

[c] Calculated from TEM

Reaction conditions of catalyst: temperature: 230 °C, H_2 flow rate At. Pressure: 140 mL/min, WHSV: 2.09 h^{-1}

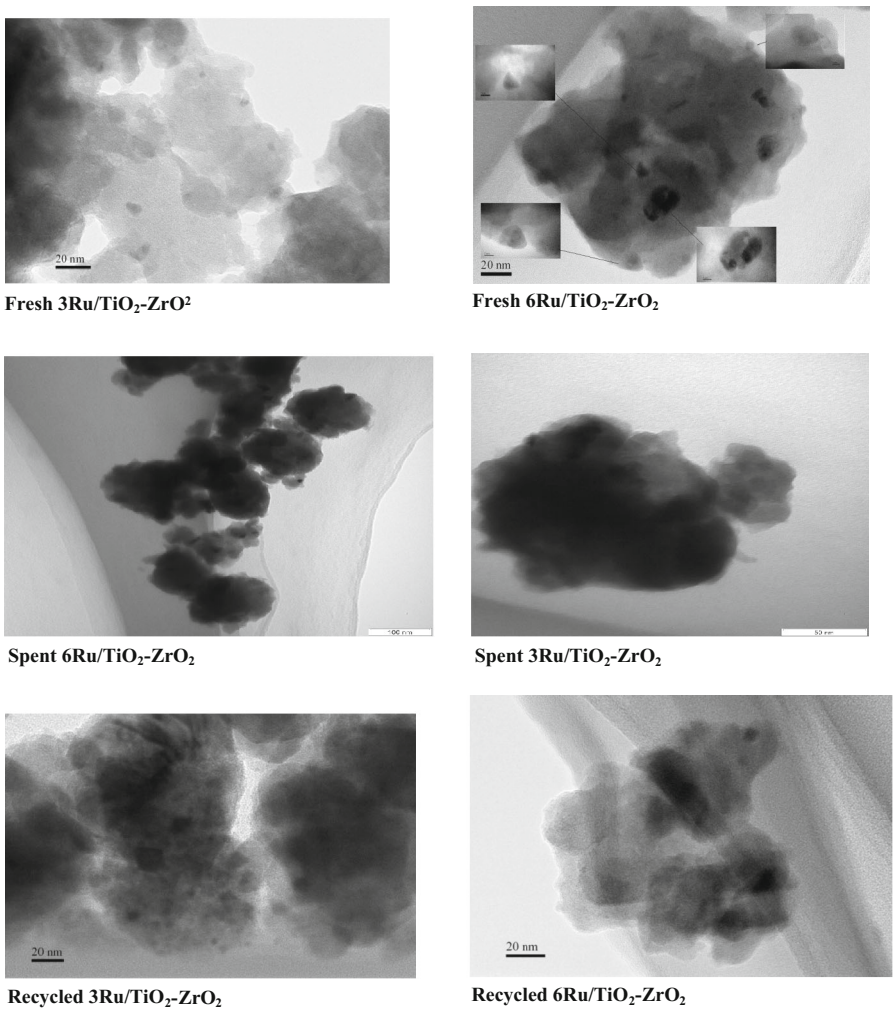

Fig. 13 TEM images of fresh, spent and recycled 3Ru/TiO_2–ZrO_2 catalysts and 6Ru/TiO_2–ZrO_2 catalysts

sort of metal activation affect such as in situ reduction occurred during the repeated reaction.

The used catalysts were characterized by TEM, BET surface area and the results were compared with values of the fresh catalysts in Figs. 12, 13 and Table 6. The TEM patterns and their particle sizes of the fresh, used and recycled catalysts are presented in Fig. 13 and Table 6. Both fresh and recycled catalysts showed similar TEM

Table 6 Spent catalyst BET- surface area analysis and particle size measured from TEM patterns

Spent catalyst	BET surface area (m^2/g) spent	Particle size (nm) spent
3Ru/TiO_2–ZrO_2	135 (147)	15.5 (14.0)
6Ru/TiO_2–ZrO_2	40 (67)	27.0 (22.0)

In parenthesis, same fresh catalyst BET- surface area and particle size from TEM patterns

Table 7 Data of the coke deposited on the catalyst analyzed by a CHNS analyzer

S.No	Catalyst	C %	H %	H/C
01	1Ru/TiO_2–ZrO_2	3.86	1.23	0.31
02	3Ru/TiO_2–ZrO_2	4.32	2.97	0.68
03	5Ru/TiO_2–ZrO_2	5.11	1.42	0.27
04	6Ru/TiO_2–ZrO_2	5.43	1.55	0.28

patterns. This suggests that the catalyst structural features were intact during the reaction. The fresh and used catalysts of 3 and 6Ru/TiO_2–ZrO_2 showed change in particle size, surface area and TEM patterns. This suggests that the structural features of 3Ru/TiO_2-ZrO_2 catalysts were intact during the reaction whereas structural features of 6Ru/TiO_2–ZrO_2 catalyst slightly varied. These findings showed that the activity of 3Ru/TiO_2–ZrO_2 was increased during repeated reaction due to the formation of active particle of metallic ruthenium. There was no indication of any agglomeration during the glycerol hydrogenolysis in the 3Ru/TiO_2–ZrO_2 catalyst. These results further suggest that the structural stability of the 3Ru/TiO_2–ZrO_2 catalyst did not affect under the glycerol hydrogenolysis conditions and 6Ru/TiO_2–ZrO_2 catalyst showed no structural stability due to the agglomeration.

The carbonaceous species formed on the catalysts are analyzed by a CHN analyzer and the results are listed in Table 7. Considerable amounts of carbon deposits were formed on the catalysts during the catalytic reaction. The textural property of the catalyst plays also an important role in coking. Table 7 shows the amount of coke accumulated on the catalysts after reaction at 230 °C. A lower coke deposition was found on 3Ru/TiO_2–ZrO_2 catalyst and even much lower coke loadings were detected on 1Ru/TiO_2–ZrO_2 compared to 6Ru/TiO_2–ZrO_2 catalyst due to the agglomeration. The carbon percentage of the carbonaceous deposits formed on 5Ru/TiO_2–ZrO_2 (5.11) and 6Ru/TiO_2–ZrO_2 (5.43) are higher than the 3Ru/TiO_2–ZrO_2 (4.32) catalyst. The large difference in the amount of coke deposits and in the H/C ratios appears to correlate with the effective pore widths and particle size of the catalysts. 6Ru/TiO_2–ZrO_2 catalysts have shown more carbonaceous deposits than the other catalysts, indicating the agglomeration of the active sites. As can be seen from the Table 7, a decrease in the surface areas and particle size has been

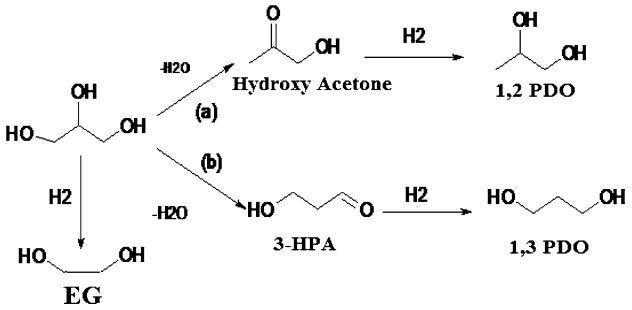

Scheme 1 Reaction scheme

observed in used catalysts, than those of the fresh catalysts. This may be due to pore blockage during the glycerol hydrogenolysis reaction which leads to deactivation of the catalyst. From Table 7, it is quite interesting to note that the average particle size and surface area greatly decreased in case of 5 and 6Ru/TiO_2–ZrO_2 catalysts in comparison to the other catalysts. This might be due to small pores easily covered by the coke deposits and is well correlated by the CHN analysis (Scheme 1).

Conclusions

Ruthenium catalysts supported on TiO_2–ZrO_2 are found to be highly active and selective for the hydrogenolysis of glycerol to propanediols. Catalysts prepared by the DP method showed good conversions as well as selectivity for the hydrogenolysis of glycerol. Low Ru content is sufficient to achieve maximum conversion if the catalysts were prepared by the DP method. The TiO_2–ZrO_2 support provides a platform for good dispersion of nano size Ru particles, which are responsible for high catalytic properties. However, as ruthenium loading increases the selectivity

towards the 1,2-propanediol, 2-propanol, 1,3–propanediol and 1-propanol increases. The varying intrinsic activity of active Ru sites nicely correlates with metal particle size. CO chemisorption, TEM studies and TPR results further suggest that the reducibility of ruthenium increases with ruthenium loading and exhibit strong metal–support interaction (SMSI) at lower ruthenium loadings. Higher activity and selectivity can be realized with $3Ru/TiO_2$–ZrO_2 catalyst due to the presence of more acidic sites which is evidenced from NH_3 to TPD results. The decrease in the conversion and selectivity of higher loading $6Ru/TiO_2$–ZrO_2 can be attributed to the agglomerisation of active Ru particles as evidenced from the BET surface area analysis, and TEM studies. Formation of carbonaceous species on the surface results in loss of active sites and also decreases of catalytic activity. Further, the conversion of glycerol and the selectivity to hydrogenolysis products 1,2-propanediol, 1,3-propanediol also depend on the reaction time and catalyst loadings. The spent catalysts (3 and $6Ru/TiO_2$–ZrO_2) were also characterized by BET surface area and TEM analysis. These results show that there is a significant decrease in the active sites of the $6Ru/TiO_2$–ZrO_2 spent catalyst which resulted a decrease in the conversion and selectivity of the catalyst.

Acknowledgments The authors thank Council of Scientific & Industrial Research, New Delhi, India and Director, CSIR-IICT, Hyderabad for her encouragement.

References

1. Zhou CH, Beltramini JN, Fan YX, Lu GQ (2008) Chemoselective catalytic conversion of glycerol as a biorenewable source to valuable commodity chemicals. Chem Soc Rev 37:527–549
2. Miyazawa T, Koso S, Kunimori K, Tomishige K (2007) Glycerol hydrogenolysis to 1,2-propanediol catalyzed by a heat-resistant ion-exchange resin combined with Ru/C. Appl Catal A Gen 329:30–35
3. Fernando S, Adhikari S, Chandrapal C, Murali N (2006) Biorefineries: current status, challenges, and future direction. Energy Fuels 20:1727–1737
4. Hamzah N, Nordin NM, Nadzri AHA, Nik YA, Kassim MB, Yarmo MA (2012) Enhanced activity of Ru/TiO_2 catalyst using bisupport, bentonite-TiO_2 for hydrogenolysis of glycerol in aqueous media. Appl Catal A Gen 420:133–141
5. Miyazawa T, Koso S, Kunimori K, Tomishige K (2007) Development of a Ru/C catalyst for glycerol hydrogenolysis in combination with an ion-exchange resin. Appl Catal A Gen 318:244–251
6. Zhu S, Gao X, Zhu Y, Zheng H, Li Y (2013) Promoting effect of boron oxide on Cu/SiO_2 catalyst for glycerol hydrogenolysis to 1,2-propanediol. J Catal 303:70–79
7. Furikado I, Miyazawa T, Koso S, Shimao A, Kunimori K, Tomishige K (2007) Catalytic performance of Rh/SiO_2 in glycerol reaction under hydrogen. GreenChem 9:582–588
8. Miyazawa T, Kusunoki Y, Kunimori K, Tomishige K (2006) Glycerol conversion in the aqueous solution under hydrogen over Ru/C+ an ion-exchange resin and its reaction mechanism. J Catal 240:213–221
9. Chaminand J, Djakovitch LA, Gallezot P, Marion P, Pinel C, Rosier C (2004) Glycerol hydrogenolysis on heterogeneous catalysts. Green Chem 6:359–361
10. Zhua S, Qiuc Y, Zhua Y, Haod S, Zhengd H, Li Y (2013) Hydrogenolysis of glycerol to 1,3-propanediol over bifunctional catalysts containing Pt and heteropolyacids. Catal Today 212:120–126
11. Dasari MA, Kiatsimkul PP, Sutterlin WR, Suppes GJ (2014) Low-pressure hydrogenolysis of glycerol to propylene glycol. Appl Catal A Gen 281:225–231
12. Pavan Kumar V, Srikanth ChS, Nageswara Rao A, Chary KVR (2014) Vapour phase hydrogenolysis of glycerol over nano Ru/SBA-15 catalysts on the effect of preparatory routes and metal precursors. JNN 143:137–3146
13. Pavan Kumar V, Kumar A, Srinivasa Rao G, Chary KVR (2015) Vapor-phase hydrogenolysis of glycerol over nanostructured Ru/MCM-41 catalysts. Catal Today 250:226–238
14. Pavan Kumar V, Harikrishna Y, Nagaraju N, Chary KVR (2014) Characterization and reactivity of TiO_2 supported nano ruthenium catalysts for vapour phase hydrogenolysis of glycerol. Indian J Chem A 53:516–523
15. Feng Y, Yin H, Wang A, Shen L, Yu L, Jiang L (2011) Gas phase hydrogenolysis of glycerol catalyzed by Cu/ZnO/MOx ($MOx = Al_2O_3$, TiO_2, and ZrO_2) catalysts. Chem Eng J 168:403–412
16. Vasiliadou ES, Heracleous E, Vasalos IA, Lemonidou AA (2009) Ru-based catalysts for glycerol hydrogenolysis-effect of support and metal precursor. Appl Catal B Environ 92:90–99
17. Chary KVR, Vidya Sagar G, Naresh D, Kalyana Seela K, Sridhar B (2005) Characterization and reactivity of copper oxide catalysts supported on TiO_2–ZrO_2. J Phys Chem B 109:9437–9444
18. Nakano Y, Hattori H, Tanabe K (1979) Surface properties of zirconium oxide and its catalytic activity for lsomerization of I-butene. J Catal 57:1–10
19. Wu JC, Chung CS, Ay CL, Wang I (1984) Nonoxidative dehydrogenation of ethylbenzene over TiO_2–ZrO_2 catalysts. J Catal 87:98–107
20. Wang I, Wu JC, Chung CS (1958) Dehydrogenation of ethylbenzene and ethylcyclohexane over mixed binary oxide catalysts containing titania. Appl Catal 16:89–101
21. Arata K, Akutagawa S, Tanabe K (1976) New solid acids and bases: their catalytic properties. Bull Chem Soc Jpn 49:390
22. Lungang C, Yulei Z, Hongyan Z, Zhang C, Li Y (2012) Catalytic degradation of aqueous Fischer–Tropsch effluents to fuel gas over oxide-supported Ru catalysts and hydrothermal stability of catalysts. J Chem Technol Biotechnol 87:1089–1097
23. Srikanth CHS, Pavan Kumar V, Viswanadham B, Chary KVR (2011) Hydrodechlorination of 1,2,4-trichlorobenzene over supported ruthenium catalysts on various supports. Catal Commun 13:69–72
24. Watanabe S, Ma X, Song C (2009) Characterization of structural and surface properties of nanocrystalline TiO_2–CeO_2 mixed oxides by XRD, XPS, TPR, and TPD. J Phys Chem C 113:14249–14557
25. Adeeva V, Lei GD, Sachtler WHM (1994) Isomerization of 13C labeled butane over Fe, Mn promoted sulfated ZrO_2 catalyst. Appl Catal A 118:L11–L15

26. Chakroune N, Viau G, Ammar S, Poul L, Veautier D, Chehimi MDM, Mangeney C, Villain F, Fievet F (2005) Acetate- and thiol-capped monodisperse ruthenium nanoparticles: XPS, XAS, and HRTEM studies. Langmuir 21:6788–6796
27. Kusunoki Y, Miyazawa T, Kunimori K, Tomishige K (2005) Highly active metal–acid bifunctional catalyst system for hydrogenolysis of glycerol under mild reaction conditions. Catal Commun 6:645–649
28. Schlaf M (2006) Selective deoxygenation of sugar polyols to a, x-diols and other oxygen content reduced materials-a new challenge to homogeneous ionic hydrogenation and hydrogenolysis catalysis. Dalton Trans 39:4645–4653
29. Dam JT, Hanefeld U (2011) Renewable chemicals: dehydroxylation of glycerol and polyols. Chem Sustain Chem 4:1017–1034
30. Martin A, Armbruster U, Gandarias I, Arias PL (2013) Glycerol hydrogenolysis into propanediols using in situ generated hydrogen—a critical review. Eur J Lipid Sci Technol 115:9–27
31. Nakagawa Y, Tomishige K (2011) Heterogeneous catalysis of the glycerol hydrogenolysis. Catal Sci Technol 1:179–190
32. Balaraju M, Rekha V, Prabhavathi Devi BLA, Prasad RBN, Sai Prasad PS, Lingaiah N (2010) Surface and structural properties of titania-supported Ru catalysts for hydrogenolysis of glycerol. Appl Catal A Gen 384:107–114
33. Quesada DE, Ortiz MIM, Jimenez JJ, Castellon ER, Lopez AJ (2006) Catalysts based on Ru/mesoporous phosphate heterostructures (PPH) for hydrotreating of aromatic hydrocarbons. J Mol Catal A 255:41–48
34. Liu Q, Guo X, Li Y, Shen W (2009) Synthesis of hollow Co structures with netlike framework. Langmuir 25:6425–6430
35. Priya SS, Kumar VP, Kantam ML, Bhargava SK, Chary KVR (2014) Vapour-phase hydrogenolysis of glycerol to 1,3-propanediol over supported Pt catalysts: the effect of supports on the catalytic functionalities. Catal Lett. doi:10.1007/s10562-014-1395-1
36. Priya SS, Kumar VP, Kantam ML, Bhargava SK, Chary KVR (2014) Catalytic performance of Pt/$AlPO_4$ catalysts for selective hydrogenolysis of glycerol to 1,3- propanediol in the vapour phase. RSC Adv 4:51893–51903